Geochemical Insights into the Paleodepositional Environment of the Garagu Formation, Gara Anticline, Kurdistan, Northern Iraq

Ibrahim M.J. Mohialdeen[1], Tola A. Mirza[1†] and Shahra O. Abdalla[2]

[1]Department of Earth Sciences and Petroleum, College of Science, University of Sulaimani, Kurdistan Region – F.R. Iraq

[2]Development Center for Research and Training, University of Human Development, Sulaymaniyah, Kurdistan Region – F.R. Iraq

***Abstract*—The Garagu Formation is mostly composed of carbonate layers with iron-rich horizons in the middle part. The geochemical evidence for the paleodepositional environment of the Garagu Formation in the Kurdistan Region of Iraq's Gara anticline has been explored in this paper. A total of 9 samples from the Garagu Formation were analyzed by XRF for major elements and inductively coupled plasma–mass spectrometer for trace elements. From geochemical data of major and trace elements, including rare earth elements, a series of identification indexes, such as Sr/Ba, Rb/K_2O, Th/U, U/Th, V/(V+Ni), δU, V/Sc, Sr/Cu, and C-Value ratios, are calculated which can be used to indicate, paleosalinity, ancient oxidizing environment, and paleoclimate conditions. As would be predicted in this limestone-dominated deposit, CaO has the greatest weight percentages of any sample. Several samples from the iron-rich mineralization in the middle part of the formation exhibit significant percentages of FeO. The elemental geochemical ratios indicate to saline shallow marine environment with lower salinity in the middle part of the formation. The paleoredox proxies revealed that the oxic to suboxic conditions are prevailed during the deposition of the formation.**

***Index Terms*—Cretaceous, Gara mountain, Garagu formation, Kurdistan, Rare earth element.**

I. Introduction

The Gara anticline in the Amedi District, Duhok Governorate, is one of the most intriguing geological regions in Kurdistan (Fig. 1). The type localities of the Baluti, Garagu, and Chia Gara formations are located in the core of the anticline (Bellen, et al., 1959, Hanna, 2007, Aljumaily and Abdulla, 2013). Wetzel was the first to study the Garagu Formation (Valanginian-Hauterivian), from its type locality (Bellen, et al., 1959). The research area's Garagu Formation comprises several limestone beds with siltstones, sandy limestones, and oolitic limestones (Mirza, Mohialdeen and Awadh, 2016, Ghafor and Mohialdeen, 2016; 2018). New paleontological studies indicated to Valanginian-Barremian age of the Garagu Formation (Amin, 1989, Ghafor and Mohialdeen, 2018). The Garagu Formation is divided into three sections reaching a maximum thickness of 92 m (Mirza, Mohialdeen and Awadh, 2016). The lower part of the Garagu Formation (46 m) consists of oolitic and coarse sandstone and sandy, oolitic limestones with a rich fauna. The middle part of the succession (22 m) includes organic detrital limestones. The top 24 m of the formation includes ferruginous oolitic marls and sandstones.

A recent sedimentological study of the Garagu Formation, conducted by (Mahdi and Al-Zaidy, 2024), examined three subsurface sections through microfacies analyses. The study revealed a diverse range of depositional environments, spanning from restricted marine to open marine, as well as mid-to outer ramp settings.

Previous studies have utilized geochemical parameters to explore the paleo-oxygenation conditions of ancient sediments (Mustafa and Tobia, 2020, Al-Juboury, et al., 2023, Yu, et al., 2023, Xiao, et al., 2024). The present study investigates the geochemistry of major and trace elements of the Garagu Formation. Specifically, it focuses on the geochemical data as evidence to infer the paleodepositional conditions of this formation. This research aims to enhance our understanding of the depositional conditions of the Early Cretaceous Garagu Formation.

II. Geological Setting

Within the High Folded Zone of northern Iraq, the Gara anticline is a double plunging fold that runs E-W for approximately 80 km in length and 12 km in breadth, parallel to the Taurus Mountains (Aljumaily and Abdulla, 2013). The High Folded Zone is between 25 and 50 km wide. In this zone, the folds are aligned with an E-W trend in northern Iraq and an NW-SE trend in northeastern Iraq. With steeper S- or SW-dipping limbs and occasionally a thrust fault in the

ARO-The Scientific Journal of Koya University
Vol. XIII, No. 1 (2025), Article ID: ARO.11910. 10 pages
DOI: 10.14500/aro.11910
Received: 22 November 2024; Accepted: 03 February 2025
Regular research paper; Published: 13 February 2025
†Corresponding author's e-mail: tola.merza@univsul.edu.iq

http://dx.doi.org/10.14500/aro.11910

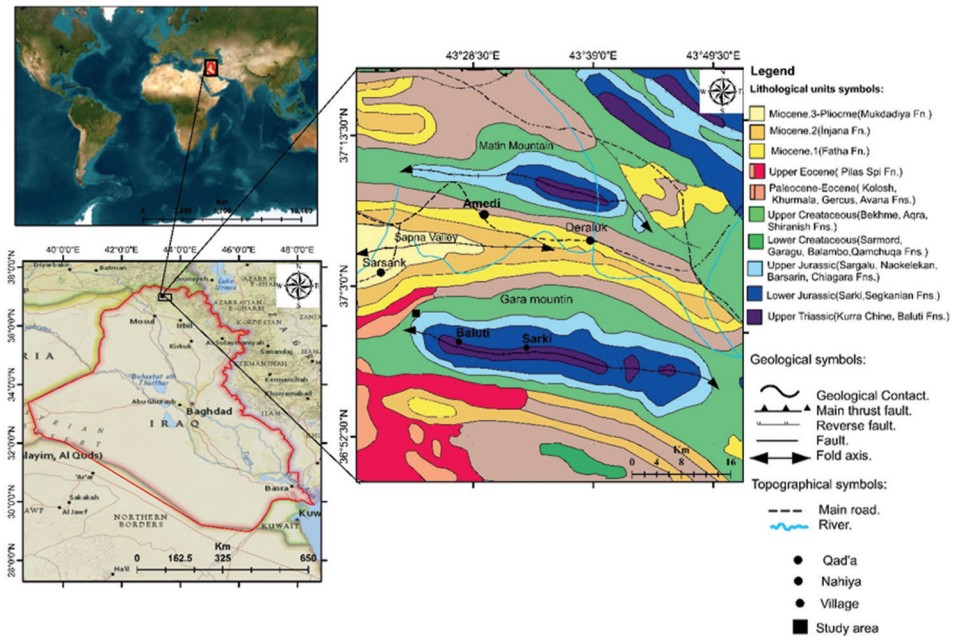

Fig. 1. Geological map of Gara anticline and the surrounding areas modified after (Hanna, 2007; Mirza, Mohialdeen and Awadh, 2016).

steeper limb, the folds are primarily asymmetrical (Jassim and Goff, 2006). The stratigraphic succession of the anticline, from the Late Triassic to the Late Miocene, is documented (Bellen, et al., 1959).

The type locality of the Garagu Formation, situated within the Gara anticline, is located approximately 600 m north of Garagu Village in the Gali Garagu Valley at coordinates N 37° 1' 06" and E 43° 23' 24.1" (Fig. 1). Differently colored limestone layers with varying faunal contents make up the succession. The beds have a 272° strike; a 62° dip angle, and a 002° dip direction. The total thickness of this section, as determined by Wetzel (Bellen, et al., 1959), is around 2 m more than the 89.9 m shown here (Fig. 2). Soil covered a tiny portion of the outcrops in the region under study (Fig. 2).

The lower contact is conformable and gradational, and it is with the Tithonian-Berriasian Chia Gara Formation (Bellen, et al., 1959). The contact occurs above the dark limestone strata of the Chia Gara Formation and at the start of the siltstone and oolitic limestone beds of the Garagu Formation. The top of the peloidal limestone and the start of the yellowish marl strata mark the gradational upper contact with the Sarmord Formation (Valanginian-Aptian) (Mirza, Mohialdeen and Awadh, 2016, Ghafor and Mohialdeen, 2018).

III. Samples and Methods

Fig. 2 displays the locations of the 20 samples that were taken from the Garagu Formation outcrop from the Gara anticline. These samples were previously studied from the paleontological points of view (Ghafor and Mohialdeen, 2016; 2018), as well as from iron mineralization within the middle part of the formation (Mirza, Mohialdeen and Awadh, 2016). The major and trace elements (including REE) contents of nine selected samples were determined using the XRF, and inductively coupled plasma–mass spectrometer (ICP-MS) techniques, respectively. Samples were prepared (dissolved in acid and filtering) and measurements were taken at Washington State University, School of Environmental Science, USA. By performing repeated analyses of samples and laboratory standards, reproducibility and accuracy were verified.

All samples' measured REE contents were normalized to Post-Archean Australian Shale (PAAS, Taylor and McLennan, 1985). The equations listed as follows: (i) $\delta Eu= Eu_N/(Sm_N*Gd_N)^{0.5}$, and (ii) $\delta Ce= 3Ce_N/(2La_N+Nd_N)$ have been used to test whether a real Eu and Ce anomalies exist (Bau and Dulski, 1996; MacLeod and Irving, 1996; Shields and Stille, 2001; Lawrence, et al., 2006; Ozyurt, Kirmaci and Al-Aasm, 2019; Ozyurt, et al., 2020; Mirza, et al., 2021; Xu, et al., 2023; Xiao, et al., 2024). The following formula is also used to determine the authigenic uranium (δU): $\delta U = U/[0.5 \times (Th/3 + U)]$ (Yu, et al., 2023).

IV. Results

A. Major Elements

Table I reports the major oxide component of the Garagu Formation. In general, the analyzed samples from the Garagu Formation have high CaO content (32.42–52.96%). SiO_2 content and other oxides are greatly diluted by such content (2.37–8.98%), Al_2O_3 (0.39–3.82%), FeO (0.95–19.73%), MgO (0.39–3.77%), Na_2O (0.01–0.03%), K_2O (0.05–0.46%), MnO (0.025–0.085%), TiO_2 (0.032–0.262%), and P_2O_5 (0.005–0.174%). In comparison to the PAAS, the examined samples exhibit depletion in every element except CaO and FeO (Fig. 3). The CaO enrichment in these samples indicates the calcium carbonate composition of the rocks. The high occurrence of iron mineralization in the Garagu Formation, especially the middle part (Mirza, Mohialdeen and Awadh, 2016) is the consequence of the high occurrence of FeO (Table I and Fig. 3).

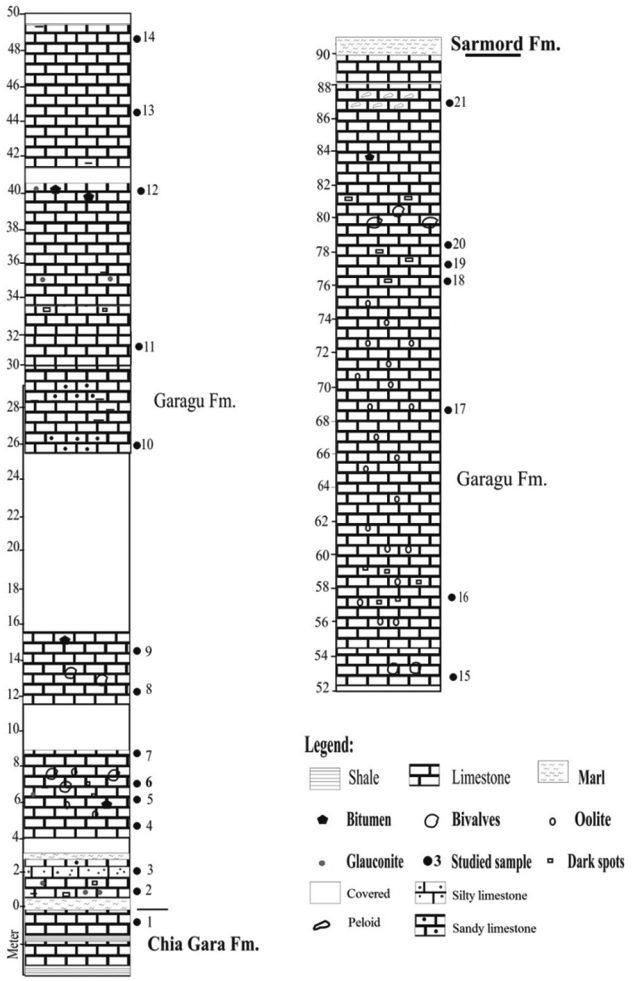

Fig. 2. Garagu Formation stratigraphic column, Gara Anticline, Amedi District, Duhok Governorate, Kurdistan, after (Mirza, Mohialdeen and Awadh, 2016).

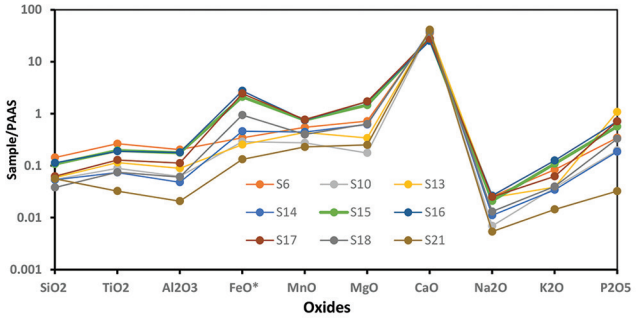

Fig. 3. PAAS-normalized diagram for major oxides of the Garagu Formation PAAS values after (Taylor and McLennan, 1985).

B. Trace Elements

Table II lists the trace element composition of the Garagu Formation. In comparison to PAAS, the examined samples exhibit depletion in almost all other elements and enrichment in Sr and, in certain cases, V (Fig. 4).

C. Rare Earth Elements (REE)

Table III indicates the low content of REE in the analyzed samples. A variety of REE characteristics may be calculated

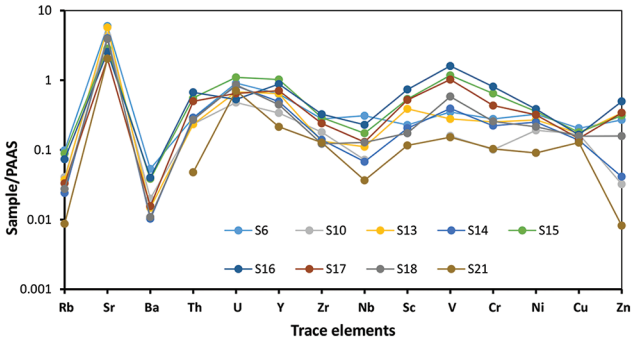

Fig. 4. PAAS-normalized diagram for trace elements of the Garagu Formation PAAS value after (Taylor and McLennan, 1985).

to characterize the enrichment and origins of REE, reflecting geochemical properties (Table IV). The content of total REEs (ΣREE) in the studied samples from the Garagu Formation ranged from 19.57 ppm to 132.38 ppm (average = 80.04 ppm), significantly lower than for upper continental crust (UCC; 146.37 ppm) and (PAAS;184.77 ppm) (Table IV and Fig. 5).

The REE patterns are enriched in MREE relative to LREE and HREE, in other words, it has a bell shape, which is due to the iron oxides enrichment (Fig. 5). However, there is a small difference between the patterns of the study samples and UCC, but still indicating that the source of sediments in Garagu Basin mainly comes from the upper crust. La/Yb -∑REE diagram of the Garagu Formation indicates the sedimentary rocks origin of these sediments (Fig. 6).

V. Discussion

A. General Distribution of ELEMENTs

A substantial correlation of −0.563 between ΣREE and CaO suggests that the main control on the REE concentrations is the effect of dilution by carbonate materials (Table V). The enrichment of the samples with Sr indicates the association with the carbonate phase, especially calcite mineral (Mustafa and Tobia, 2020; Ozyurt, et al., 2020). Furthermore, there is a clear link between the ΣREE and SiO_2, Al_2O_3, and total FeO (0.549, 0.737, and 0.429, respectively, Table V) suggest the typical role of clay minerals on the distribution of REEs (Mclennan, 2018; Condie, 1991). The variation in the total REE concentration of the Garagu Formation (Table IV) indicates that the Early Cretaceous sediments' geochemical circumstances varied to some degree. The degree of difference between the light and heavy REEs in the samples may be determined by looking at the ratio of light REEs (LREE) to heavy REEs (HREE) content (Ozyurt, Kirmaci and Al-Aasm, 2019; Xiao, et al., 2024). The ratio of LREE/HREE in the Garagu Formation ranged between 4.57 and 8.14 which is much lesser than the LREE/HREE value of 9.49 in the PAAS (Taylor and McLennan, 1985). This indicates enrichment with LREE and a relative loss of HREE. However, this result does not coincide with the pattern, which is enriched in MREE (Fig. 5). Regarding the iron-rich samples (i.e. S15, S16, and S17), they are generally enriched with ΣREE (Table IV); however, no significant correlation (+0.429) between FeO and ΣREE content is present (Table V).

The studied limestone beds have variable ΣREEs (19.57–132.38 ppm and avg. 80.04 ppm), Y (5.80–27.66 ppm; avg. 15.24 ppm), and Ho (0.17–1.1; avg. 0.60 ppm) contents.

 http://dx.doi.org/10.14500/aro.11910

TABLE I
Major Oxide Contents (wt. %) for the Garagu Formation After (Mirza, Mohialdeen and Awadh, 2016); Compared with PAAS (Taylor and McLennan, 1985)

Sample ID	SiO_2	TiO_2	Al_2O_3	FeO*	MnO	MgO	CaO	Na_2O	K_2O	P_2O_5	LOI	Total
S6	8.98	0.262	3.82	2.46	0.060	1.58	45.30	0.03	0.31	0.055	36.87	99.72
S10	3.38	0.088	1.16	2.08	0.030	0.39	51.02	0.01	0.14	0.031	40.95	99.28
S13	3.68	0.114	1.67	1.82	0.048	0.75	51.10	0.03	0.14	0.174	40.37	99.90
S14	3.33	0.073	0.90	3.30	0.049	1.36	49.27	0.01	0.13	0.030	41.40	99.86
S15	6.70	0.194	3.33	15.12	0.083	3.20	35.79	0.02	0.40	0.091	34.56	99.50
S16	7.06	0.188	3.37	19.73	0.083	3.72	32.42	0.03	0.46	0.114	32.89	100.06
S17	3.89	0.127	2.10	17.53	0.085	3.77	35.82	0.03	0.23	0.114	36.24	99.94
S18	2.37	0.074	1.13	6.75	0.044	1.39	47.87	0.02	0.15	0.053	39.73	99.57
S21	3.48	0.032	0.39	0.95	0.025	0.55	52.96	0.01	0.05	0.005	41.33	99.78
PAAS	62.4	0.99	18.78	7.18	0.11	2.19	1.29	1.19	3.68	0.16	6	103.97

FeO*: Total FeO, LOI: Loss on ignition

TABLE II
Trace element Concentrations (ppm) for the Garagu Formation; Compared with PAAS (Taylor and McLennan, 1985)

Sample ID	Large ion lithophile elements			High-field strength elements					Transition elements					
	Rb	Sr	Ba	Th	U	Y	Zr	Nb	Sc	V	Cr	Ni	Cu	Zn
S6	15.77	1194.68	34.73	4.24	2.83	17.19	58.70	5.89	3.65	52.38	30.61	17.89	10.24	22.95
S10	6.51	856.23	13.03	3.43	1.49	9.14	37.77	1.37	0.00	23.89	11.09	10.51	8.46	2.74
S13	5.97	1145.77	9.61	3.40	2.11	17.34	28.05	2.11	6.21	41.82	27.76	14.88	8.67	28.93
S14	3.87	805.47	6.68	4.22	2.58	13.35	29.32	1.29	3.28	58.92	24.48	13.82	6.91	3.51
S15	14.24	569.27	24.96	8.12	3.41	27.66	61.38	3.30	8.59	176.34	70.98	19.54	8.95	26.49
S16	11.77	508.76	26.01	9.77	1.65	23.78	68.25	4.36	11.77	240.84	89.11	21.19	8.24	42.26
S17	5.30	408.00	10.12	7.30	2.00	19.07	50.55	2.47	8.36	153.50	47.67	17.54	7.30	28.96
S18	4.41	779.64	7.08	3.94	2.67	12.06	25.71	2.44	2.78	87.58	28.30	11.83	7.89	13.46
S21	1.39	406.12	0.00	0.70	2.20	5.80	26.74	0.70	1.86	22.85	11.37	4.99	6.38	0.70
PAAS	160.00	200.00	650.00	14.60	3.10	27.00	210.00	19.00	16.00	150.00	110.00	55.00	50.00	85.00
LDL.	0.2	0.1	0.5	0.1	0.1	0.5	2.0	0.2	1.6	5.0	3.0	3.5	5.0	0.3

TABLE III
Rare Earth Element concentrations (ppm) for Selected Samples of the Garagu Formation, Duhok Governorate, Kurdistan, Iraq

Sample	Thickness (m)	La	Ce	Pr	Nd	Sm	Eu	Gd	Tb	Dy	Ho	Er	Tm	Yb	Lu
S6	7.00	20.48	41.99	5.41	22.15	4.62	1.07	4.34	0.66	3.71	0.71	1.83	0.25	1.48	0.23
S10	26.00	8.49	16.35	2.15	8.83	1.84	0.40	1.65	0.25	1.36	0.26	0.65	0.09	0.51	0.08
S13	44.50	17.47	43.68	5.78	24.93	5.48	1.18	4.76	0.66	3.37	0.60	1.40	0.18	0.99	0.14
S14	48.50	11.23	27.25	3.50	14.74	3.37	0.77	3.17	0.47	2.57	0.47	1.13	0.15	0.84	0.13
S15	52.50	20.18	49.41	6.37	27.33	6.93	1.68	7.12	1.10	5.96	1.10	2.66	0.35	1.91	0.28
S16	57.50	11.19	28.20	3.57	14.80	3.89	0.92	4.09	0.70	4.02	0.76	1.96	0.28	1.65	0.24
S17	69.00	16.99	40.34	5.06	21.59	5.32	1.27	5.43	0.87	4.84	0.91	2.23	0.29	1.77	0.26
S18	76.40	8.41	20.15	2.57	10.86	2.66	0.60	2.62	0.39	2.17	0.40	0.95	0.12	0.70	0.10
S21	87.20	3.37	6.89	0.97	4.08	0.97	0.22	0.97	0.15	0.87	0.17	0.44	0.06	0.35	0.05
PAAS		38.20	79.60	8.83	33.90	5.55	1.08	4.66	0.77	4.68	0.99	2.85	0.41	2.82	0.43
UCC		30.00	64.00	7.10	26.00	4.50	0.88	3.80	0.64	3.50	0.80	2.30	0.33	2.20	0.32

TABLE IV
REE Geochemical Characters of the Garagu Formation, Duhok Governorate, Kurdistan, NE Iraq

S.No.	Thickness (m)	∑REE	LREE	HREE	Sm/Yb	L/H	Y/Ho	Eu/Sm	$(Nd/Yb)_N$	$(Pr/Yb)_N$	δCe	δEu	δPr	δLa	δU
S6	7.00	108.93	95.72	13.21	3.12	7.25	27.69	0.23	1.24	1.17	0.92	1.12	1.04	1.01	0.98
S10	26.00	42.90	38.06	4.85	3.58	7.85	29.39	0.22	1.43	1.34	0.87	1.07	1.05	1.06	1.10
S13	44.50	110.62	98.52	12.10	5.55	8.14	25.97	0.22	2.10	1.87	1.00	1.09	1.02	0.93	1.31
S14	48.50	69.78	60.86	8.93	4.02	6.82	26.29	0.23	1.46	1.33	1.00	1.1	1.02	0.92	1.13
S15	52.50	132.38	111.90	20.48	3.63	5.46	24.85	0.24	1.19	1.07	1.00	1.13	1.01	0.95	0.71
S16	57.50	76.26	62.57	13.70	2.36	4.57	22.47	0.24	0.75	0.69	1.04	1.09	1.02	0.86	0.77
S17	69.00	107.19	90.57	16.60	3.00	5.46	23.59	0.24	1.01	0.91	1.00	1.11	1.00	0.99	0.69
S18	76.40	52.71	45.25	7.45	3.80	6.07	26.50	0.22	1.29	1.17	1.00	1.07	1.01	0.95	1.10
S21	87.20	19.57	16.50	3.06	2.79	5.39	29.56	0.23	0.97	0.89	0.87	1.08	1.07	0.98	1.58

TABLE V
RESULTS OF CORRELATION COEFFICIENT ANALYSIS FOR THE MAJOR OXIDES AND ∑REE, FOR THE GARAGU FORMATION, DUHOK GOVERNORATE, KURDISTAN, NE IRAQ

	SiO_2	TiO_2	Al_2O_3	FeO*	MnO	MgO	CaO	Na_2O	K_2O	P_2O_5	∑REE
SiO_2	1										
TiO_2	**0.941**	1									
Al_2O_3	**0.924**	**0.982**	1								
FeO*	0.316	0.395	0.547	1							
MnO	0.558	0.675	0.771	**0.891**	1						
MgO	0.446	0.523	0.648	**0.968**	**0.960**	1					
CaO	−0.540	−0.610	−0.733	**−0.966**	**−0.954**	**−0.982**	1				
Na_2O	0.521	0.681	0.708	0.490	0.679	0.565	−0.572	1			
K_2O	**0.801**	**0.837**	**0.918**	0.764	**0.846**	0.797	**−0.883**	0.582	1		
P_2O_5	0.170	0.365	0.429	0.444	0.575	0.439	−0.442	**0.799**	0.405	1	
∑REE	0.549	0.731	0.737	0.429	0.761	0.558	−0.563	0.688	0.606	0.697	1

Bolded: Significant at 0.01 level, Underlined: Significant at 0.05, no. of samples=9

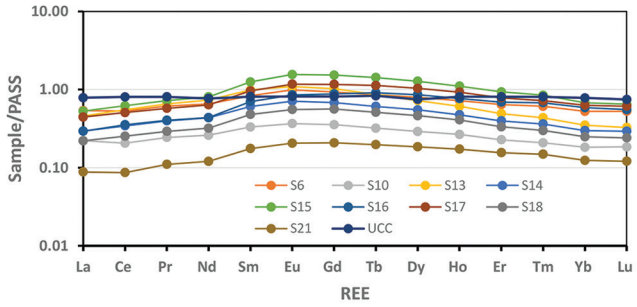

Fig. 5. PAAS-normalized REE pattern for the Garagu Formation PAAS value after (Taylor and McLennan, 1985).

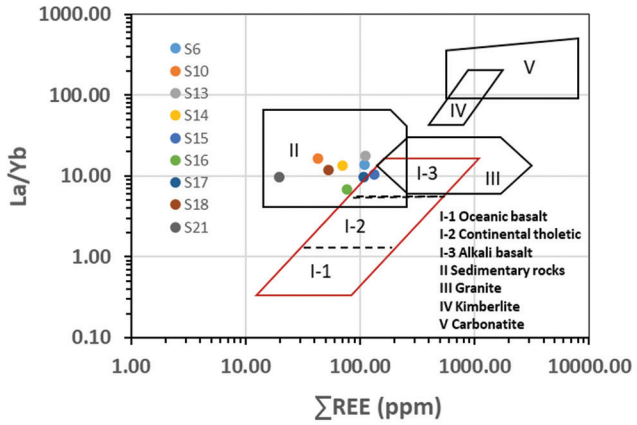

Fig. 6. La/Yb -∑REE diagram of the Garagu Formation, Duhok Governorate, Kurdistan, northeastern Iraq, the diagram after (Xiao, et al., 2024).

Their Y/Ho (22.47–29.56; ave. 26.26) and Eu/Sm (0.22–0.24; avg. 0.23) ratios are mostly similar to those of seawater while their Sm/Yb (2.36–5.55; avg. 3.54) ratios are slightly higher than those of modern seawater (Holser, 1997) (Tables II-IV).

Following normalization of REEs to PAAS (Fig. 5), the limestone samples of Garagu Formation exhibit the following properties; (i) slightly enriched of LREE relative to HREE (Table IV), $(Nd/Yb)_N$ (0.75–2.1; 1.27 avg.), and $(Pr/Yb)_N$ (0.69–1.87; 1.16) (ii) slightly negative δCe (0.87–1.04; ave. 0.97) (Murray, et al., 1991) slight positive δEu (1.07–1.13; avg. 1.10), (iv) slightly flat δPr (1.00–1.07; avg. 1.03) anomalies, and (v) slightly negative to flat δLa anomaly (0.86–1.06; avg. 0.96).

The REE content of the Garagu Formation sediments in the studied section could be useful for determining or estimating several depositional and post-depositional conditions in which the sediments are affected by them. In this section, some influences and properties will be discussed.

B. Effect of Diagenesis

These carbonate rocks of the Garagu Formation may be subjected to a diagenetic process at different levels. The influence of the diagenetic process on REE content may be deduced using the REE-analyzed data (Ozyurt, et al., 2020; Xiao, et al., 2024). Shields and Stille (2001) suggested that the diagenetic process may affect the presence of Ce and Eu related to total REE. They determined that the aberrant Ce values and the correlation between δCe and δEu can be altered by diagenesis. They concluded that the diagenesis impact results from a good positive correlation between δCe and ∑REE, and a good negative correlation between δCe and δEu. The cross plot of δCe and ∑REE for the Garagu Formation samples indicates to a slightly positive correlation between δCe and ∑REE with R^2= 0.3 (Fig. 7a). The link between δCe and δEu (with R^2 = 0.09) in the same sediments is weak or not significant (Fig. 7b). On the other hand, δEu values over 1 may suggest either diagenetic impacts on the REE characteristics or contamination from detrital input to the basin (Murray, et al., 1991; Abedini and Calagari, 2015; Ozkan, 2019). Fig. 7a and b, together with Table IV, indicate that diagenesis has little impact on the REE geochemical characteristics of the Garagu Formation samples, which predominantly reflect their original sedimentary attributes.

Two crucial factors in REE interpretations are δEu and δCe, which show the anomalous degree of δEu and δCe, respectively. Eu remains in a positive trivalent state within the oxidation environment (Tribovillard, et al., 2006; Xiao, et al., 2024). As mentioned previously, the δEu values are around 1.0 (Table IV) indicating a slightly positive anomaly. Ce typically has two valence states, Ce^{3+} and Ce^{4+}, as a result of ambient redox conditions and pH variations. In the oxidizing environment, Ce^{3+} will be oxidized to Ce^{4+}, increasing the concentration of Ce^{4+} in sediments and an enrichment of Ce in sediments (Xiao, et al., 2024). Ce can be used in the reconstruction of paleoredox conditions in the oceans (e.g. Pattan, et al., 2005; Tostevin, et al., 2016).

http://dx.doi.org/10.14500/aro.11910

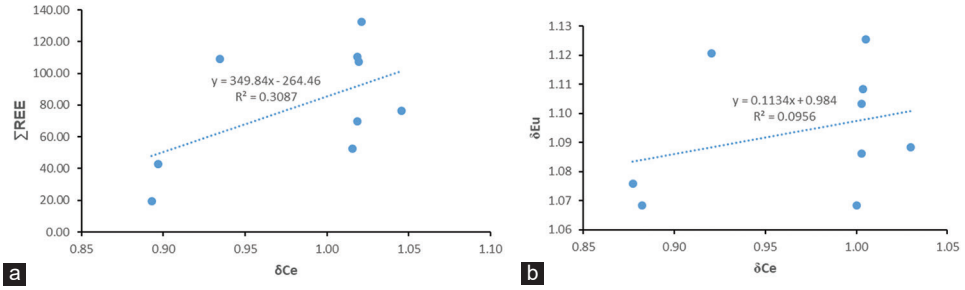

Fig. 7. Bivariate plots for δCe versus ∑REE (a) and δCe versus δEu (b) of the Garagu Formation, Duhok Governorate, Kurdistan, NE Iraq.

Craigie (2018) concluded that Ce is relatively depleted in anoxic sediments which show a negative δCe. Besides, it has been suggested that a pronounced negative δCe can be divided into three categories: (a) smaller than 0.5; (b) ~0.6–0.9, and (c) ~0.9–1.0 which represents, oxic, suboxic, and anoxic marine water, respectively (Chen, et al., 2015). Regarding the studied Garagu samples, they reveal a weak negative anomaly (Fig. 5 and Table IV) (δCe values range from 0.87 to 1.04, an average of 0.98), indicating anoxic conditions during the deposit of Garagu sediments. The Garagu Formation's water environment was comparatively constant during the sedimentation period, as evidenced by the narrow range of vertical values for δEu and δCe. However, a small difference was noted within the middle part of the formation (S15, S16, and S17) (Table IV). Ce concentrations may not be a good indicator of paleoredox where whole-rock analysis is undertaken on field samples, because the Ce is also concentrated in detrital siliciclastic minerals, so positive or negative δCe may simply reflect variations in the proportion of this material rather than any changes in paleoredox (Wilde, Quinby-Hunt and Erdtmann, 1996).

The Garagu limestones have Y/Ho values ranging between 22.47 and 29.56 (average 26.25). This suggests that the Garagu carbonates' Y/Ho levels reflect terrestrial rather than marine entry (Ozkan, 2019). The absence of correlation between δEu and δCe (Fig. 7b) suggests a negligible or absence of influence of post-depositional alteration on the measured δCe (Ozyurt, et al., 2020). In addition, this relationship indicates the terrestrial effect rather than the diagenetic effect for REEs (Ozkan, 2019). Although interference with Ba during ICP-MS analysis can taint δEu (Tostevin, et al., 2016), δEu values show no correlation with Ba/Sm, suggesting that utilized anomalies are genuine positive Eu anomalies (Fig. 8).

C. Paleosalinity Indicators

Since the sedimentary circumstances of the environment will influence the distribution of major, trace, and REEs within a column of sediments, the REE characteristics can be utilized as an indicator for the sedimentary environment (McLennan and Taylor, 1984; Mustafa and Tobia, 2020; Omar, et al., 2022; Omar, et al., 2020; Yu, et al., 2023). Three of these ratios (i.e. Sr/Ba, Rb/K_2O, and Th/U) were used to deduce the paleosalinity of the water during the deposition of Garagu Formation.

Sr/Ba

In diverse sedimentary settings, strontium (McLennan and Taylor, 1984) and barium (Ba) display distinct geochemical behaviors (Randive, 2013). The Sr/Ba ratio is widely regarded as an empirical indicator of paleo-salinity (Omar, et al., 2022; Yu, et al., 2023; Al-Taee, et al., 2024). A high Sr/Ba ratio reflects high salinity, and/or arid climate, while a low Sr/Ba ratio indicates low salinity and/or humid climate (Mohialdeen and Raza, 2013; Wang, et al., 2020; Mirza, et al., 2021; Omar, et al., 2022). The Sr/Ba ratio in the studied samples ranges between 0.00 and 120.63; (Table VI and Fig. 9) indicating some change in salinity and/or aridity of the climate. The lower and upper parts mostly show a high ratio, which indicates high salinity and/or arid climate, while the middle part (S15, S16, and S17) show low values (22.81, 19.56, and 40.3) indicate to low salinity and/or humid climate**.**

Rb/K_2O

Since the values of Rb and K are not in the same order of magnitude, it is required to expand the Rb/K_2O values by 1000 times. This makes Rb/K_2O another popular indication of paleosalinity in sedimentary areas: When the Rb/K_2O value of the water body is >6, it is the saline sedimentary environment, 4□6 is brackish water sedimentary environment, and <4 is the freshwater sedimentary environment (Jinhua, et al., 2018). Garagu samples had Rb/K_2O values above 20 (Table VI and Fig. 9). In general, it shows that the saline marine environment is the basin condition of the Garagu Formation.

Th/U

The Th/U ratio is a useful indicator for differentiating between continental and marine deposits. In general, a water body is considered to be in a terrestrial freshwater habitat when its Th/U value is more than 7, a brackish water sedimentary environment when it is between 2 and 7, and a marine saline water environment when it is <2 (Zhang, et al., 2008). Th/U values of the Garagu samples are <2, except for four samples with more than 2) (Table VI and Fig. 9). Hence, the Th/U ratios indicate to saline marine/brackish water environments.

D. Paleoredox Environment

Redox-sensitive components are thought to be a helpful technique for identifying sediment deposition in both marine and non-marine settings. Redox conditions primarily

TABLE VI
PALEOENVIRONMENTAL SENSITIVE RATIOS FOR BEDS OF GARAGU FORMATION FROM DUHOK GOVERNORATE, KURDISTAN, N IRAQ

S. No.	Thickness(m)	Sr/Ba	Rb/K_2O	Th/U	U/Th	V/(V+Ni)	V/Sc	V/Cr	Rb/Sr	Sr/Cu
S6	7.00	34.40	51.22	1.50	0.67	0.75	14.35	1.71	0.01	116.66
S10	26.00	65.72	46.97	2.31	0.43	0.69	0.00	2.15	0.01	101.24
S13	44.50	119.28	42.06	1.61	0.62	0.74	6.74	1.51	0.01	132.18
S14	48.50	120.63	30.65	1.64	0.61	0.81	17.96	2.41	0.00	116.54
S15	52.50	22.81	35.55	2.38	0.42	0.90	20.52	2.48	0.03	63.63
S16	57.50	19.56	25.49	5.93	0.17	0.92	20.46	2.70	0.02	61.74
S17	69.00	40.30	23.17	3.65	0.27	0.90	18.37	3.22	0.01	55.90
S18	76.40	110.18	30.25	1.48	0.68	0.88	31.46	3.09	0.01	98.84
S21	87.20	0.00	26.25	0.32	3.17	0.82	12.31	2.01	0.00	63.65

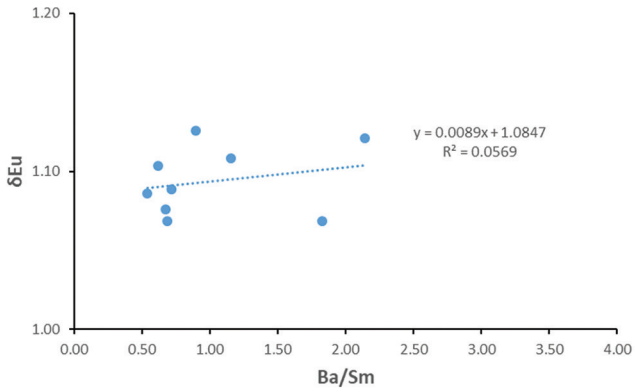

Fig. 8. Plot of Ba/Sm versus δEu ratios of studied limestone samples from the Garagu Formation.

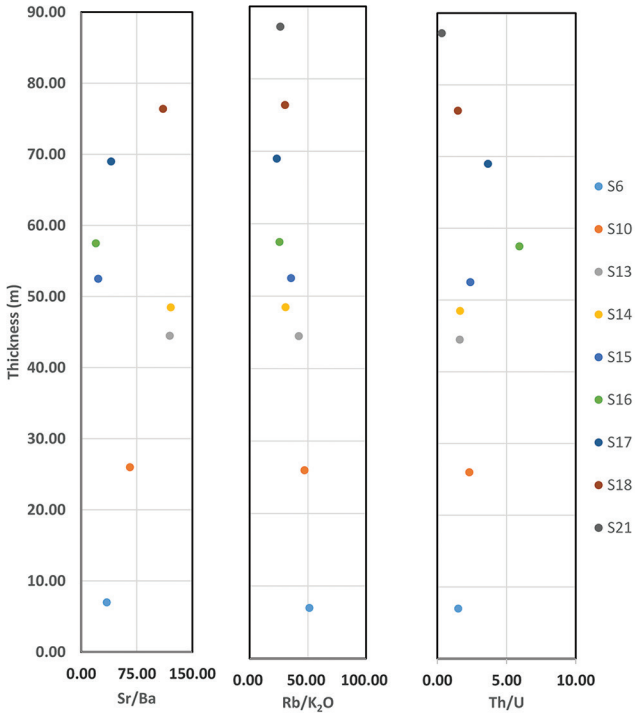

Fig. 9. Chemostratigraphy profile of Sr/Ba, Rb/K_2O, and Th/U ratios in Garagu Formation, Kurdistan, N Iraq.

govern the mobilization, precipitation, and concentration of these multivalence elements, which are abundant in anoxic sediments and include V, U, Ni, Cr, and Mo (Mustafa and Tobia, 2020; Al-Juboury, et al., 2023; Xiao, et al., 2024; Yu, et al., 2023). Furthermore, the ratios of these elements (U/Th, V/Cr, and V/Sc) have been used to estimate the paleoredox condition (Mirza, Mohialdeen and Awadh, 2016; Tobia and Shangola, 2016; Al-Taee, et al., 2024). It may be possible to differentiate between the different depositional conditions (oxic, suboxic, and anoxic) by using trace elements and their ratios in combination.

U/Th

According to Madhavaraju, et al. (2016), the U/Th ratio is regarded as a trustworthy method for determining the oxygenation level in the deposition basin. According to McKirdy, et al. (2011), the U/Th ratio may be thought of as a redox index, with low values (<0.75) linked with oxic environments and high values (>1.25) associated with anoxic environments. The low U/Th value of the Garagu samples (<1.0, except sample No.21 with 3.17; Table VI and Fig. 10) is indicative of the oxic environments (more oxygenation conditions).

V/(V+Ni)

One of the geochemical redox indications is the V/(V+Ni) ratio. According to some theories, ratios over 0.84 signify reducing circumstances, those between 0.6 and 0.84 signify a mild oxidation–reduction environment, and those below 0.6 signify an oxygen-enriched environment (Zhang, et al., 2008; Al-Juboury, et al., 2023; Yu, et al., 2023). Furthermore, low V/(V+Ni) ratios often indicate oxic to suboxic conditions, whereas a high V/(V+Ni) value indicates anoxic bottom water conditions. Most of the studied samples have V/(V+Ni) <0.84 indicating weak oxidation-reduction conditions. The samples G15, G16, G17, and G18 have higher V/(V+Ni) ratios reflecting more anoxic conditions (Table VI and Fig. 10).

δU

Argillaceous rocks are frequently abundant in radioactive elements, such as U and Th. While the U element will be lost or exist as oxides during weathering, the Th element is readily absorbed by clay minerals and preserved (Yu, et al., 2023). Consequently, the oxidation-reduction property of the paleoenvironment may be ascertained using the authigenic uranium (δU) technique. The δU for the studied samples was calculated and the results are cited in Table IV. δU = 1 is the critical point, δU < 1 is the normal water environment, and δU > 1 is the anoxic reduction environment (Wang, et al., 2020). The Garagu Formation's δU results in the study region have

http://dx.doi.org/10.14500/aro.11910

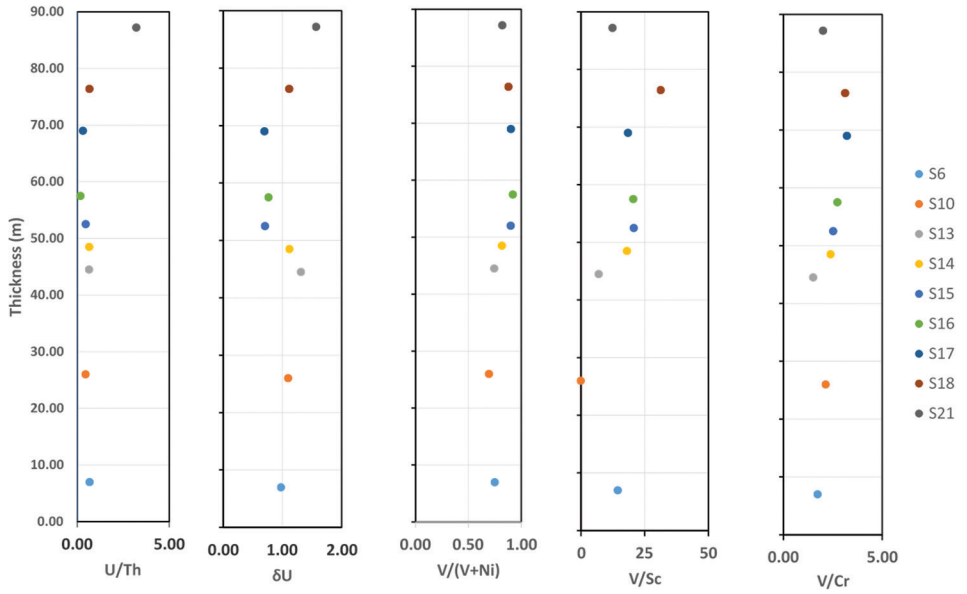

Fig. 10. Chemostratigraphy profile of U/Th, δU, V/(V+Ni), V/Sc, and V/Cr for the Garagu Formation.

an average of 1.04 and vary from 0.69 to 1.58. The Garagu sediment's δU readings indicate a mixed environment with a mild oxidizing–reduction transition.

V/Sc

According to Kimura and Watanabe (2001), who proposed V/Sc as a proxy indicator, oxidizing circumstances are indicated by V/Sc ratios <9, whereas suboxic conditions are indicated by V/Sc ratios more than 9. As seen in Table II, the Garagu samples are distinguished by their increased V/Sc values, which are greater than PAAS (9.38) and UCC (5.45). Consequently, suboxic environments are where the Garagu Formation accumulates (Fig. 10).

V/Cr

Anoxic conditions are suggested by V/Cr ratios >2, whereas stronger oxidizing circumstances are indicated by values <2 (Mustafa and Tobia, 2020; Tobia, Al-Jaleel and Ahmad, 2019; Al-Taee, et al., 2024). The V/Cr ratios for the Garagu samples are more than 2 (except two samples <2) (Fig. 10). Accordingly, the Garagu Formation is accumulated under mixed conditions oxic and anoxic conditions (or dysoxic environment).

VI. Conclusions

The elemental analysis of the Garagu Formation's type section leads to the following conclusions:

1. The remaining major and trace elements are greatly diluted by the high CaO abundance found in the Garagu Formation. The FeO data are also high and reflects the iron mineralization in the Garagu Formation, especially in the middle part of the section. Other major elements show depletion in comparison to PAAS data. The trace elements Sr, U, and V are enriched in the samples, while other trace elements show depletion.
2. The effect of the diagenetic process on REE distribution has no major effect, as deduced from the relationship between δCe and δEu, as well as from the cross plot of δCe and ∑REE in the Garagu Formation.
3. The carbonate layers formed in shallow marine high salinity to brackish water are indicated by the geochemical analyses of the Garagu Formation's main and trace elements. The range of oxic to suboxic conditions (Dysoxic) can be identified by the geochemical ratios and the contents of V, Ni, Cr, Sr, and Ba.

References

Abedini, A., and Calagari, A.A., 2015. Rare earth element geochemistry of the Upper Permian limestone: The Kanigorgeh mining district, NW Iran. *Turkish Journal of Earth Sciences*, 24, pp.365-382.

Al-Juboury, A.I., Al-Auqadi, R.S., Al-Lhaebi, S.H., Rowe, H.D., and Hussein, S.H., 2023. Anoxic marine conditions recorded from the middle Paleozoic black shales (Kaista and Ora formations), Northern Iraq: A multi-proxy approach. *Jordan Journal of Earth and Environmental Sciences*, 14, pp.50-63.

Aljumaily, I.S.I., and Abdulla, N., 2013. Inferred Inversely Reactivated Listric Faults at Chia Gara Anticline-Northern Iraq. In: *International Van Earthquake Symposium*, pp.23-27.

Al-Taee, N.T., Al-Juboury, A.I., Ghafor, I.M., Zanoni, G., and Rowe, H., 2024. Depositional environment of the late Paleocene-early Eocene Sinjar Formation, Iraq: Implications from facies analysis, mineralogical and geochemical proxies. *Heliyon*, 10, p.e25657.

Amin, D., 1989. *Biostratigraphy of Garagu Formation in Northern Iraq*. (Unpublished) M. Sc. thesis, University of Baghdad, p.14.

Bau, M., and Dulski, P., 1996. Distribution of yttrium and rare-earth elements in the Penge and Kuruman iron-formations, Transvaal Supergroup, South Africa. *Precambrian Research*, 79, pp.37-55.

Bellen, R.V., Dunnington, H., Wetzel, R., and Morton, D., 1959. *Lexique Stratigraphique International*. Vol. 3. Asie, Iraq, p.324.

Chen, J., Algeo, T.J., Zhao, L., Chen, Z.Q., Cao, L., Zhang, L., and Li, Y., 2015. Diagenetic uptake of rare earth elements by bioapatite, with an example from Lower Triassic conodonts of South China. *Earth Science Reviews,* 149, pp.181-202.

Condie, K.C., 1991. Another look at rare earth elements in shales. *Geochimica et Cosmochimica Acta*, 55, pp.2527-2531.

Craigie, N.W., 2018. Advances in oil and gas ex-ploration and production. In: Swennen, R., Ed. *Principles of Elemental Chemostratigraphy: A Practical User Guide*. Springer, Berlin, Germany. p.189.

Ghafor, I.M., and Mohialdeen, I.M., 2016. Fossils distribution from Garagu Formation (Early Cretaceous), diversity and paleoennvironmental conditions, Kurdistan Region, North Iraq. *J Zankoy Sulaimani*, Special Issue, GeoKurdistan II, pp.139-150.

Ghafor, I.M., and Mohialdeen, I.M., 2018. Early cretaceous microfossils associations (foraminifera, ostracoda, calcareous algae, and coral) from the Garagu Formation, Duhok Area, Kurdistan Region, Northern Iraq. *Arabian Journal of Geosciences*, 11, p.407.

Hanna, M., 2007. *Palynology of the Upper Part of Baluti Formation and the Nature of Its Contact with the Sarki Formation at Amadya District, NE Iraq.* PhD Thesis, Unpublished, University of Mosul, p.143.

Holser, W.T., 1997. Evaluation of the application of rare-earth elements to paleoceanography. *Palaeogeography, Palaeoclimatology, Palaeoecology*, 132, pp.309-323.

Jassim, S.Z., and Goff, J.C., 2006. *Geology of Iraq*. Vol. 5. Dolin, Prague and Moravian Museum, Brno, Czech Republic.

Jinhua, F., Shixiang, L., Liming, X., and Xiaobing, N., 2018. Paleo-sedimentary environmental restoration and its significance of Chang 7 Member of Triassic Yanchang Formation in Ordos Basin, NW China. *Petroleum Exploration and Development*, 45, pp.998-1008.

Kimura, H., and Watanabe, Y., 2001. Oceanic anoxia at the precambrian-cambrian boundary. *Geology*, 29, pp.995-998.

Lawrence, M.G., Greig, A., Collerson, K.D., and Kamber, B.S., 2006. Rare earth element and yttrium variability in South East Queensland waterways. *Aquatic Geochemistry*, 12, pp.39-72.

Macleod, K.G., and Irving, A.J., 1996. Correlation of cerium anomalies with indicators of paleoenvironment. *Journal of Sedimentary Research*, 66, pp.948-955.

Madhavaraju, J., Ramírez-Montoya, E., Monreal, R., González-León, C.M., Pi-Puig, T., Espinoza-Maldonado, I.G., and Grijalva-Noriega, F.J., 2016. Paleoclimate, paleoweathering and paleoredox conditions of lower cretaceous shales from the mural limestone, Tuape section, Northern Sonora, Mexico: Constraints from clay mineralogy and geochemistry. *Revista Mexicana de Ciencias Geológicas*, 33, pp.34-48.

Mahdi, F.A., and Al-Zaidy, A.A.H., 2024. Microfacies analysis and stratigraphic evolution of garagu formation in selected oil fields, Northern Iraq. *Iraqi Journal of Science*, 65, pp.2521-2536.

Mckirdy, D., Hall, P., Nedin, C., Halverson, G., Michaelsen, B., Jago, J., Gehling, J., and Jenkins, R., 2011. Paleoredox status and thermal alteration of the lower Cambrian (series 2) Emu Bay Shale Lagerstätte, South Australia. *Australian Journal of Earth Sciences*, 58, pp.259-272.

Mclennan, S., and Taylor, S., 1984. Archaean sedimentary rocks and their relation to the composition of the archaean continental crust. In: *Archaean Geochemistry: The Origin and Evolution of the Archaean Continental Crust.* Springer, Berlin, Germany.

Mclennan, S.M., 2018. Rare earth elements in sedimentary rocks: Influence of provenance and sedimentary processes. In: *Geochemistry and Mineralogy of Rare Earth Elements.* De Gruyter, Berlin, Germany.

Mirza, T.A., Karim, K.H., Ridha, S.M., and Fatah, C.M., 2021. Major, trace, rare earth element, and stable isotope analyses of the triassic carbonates along the Northeastern Arabian Plate margin: A key to understanding paleotectonics and paleoenvironment of the Avroman (Biston) limestone formation from Kurdistan region, Northeastern Iraq. *Carbonates and Evaporites*, 36, p.66.

Mirza, T.A., Mohialdeen, I.M., and Awadh, S.M., 2016. Iron mineralization in the Garagu Formation of Gara Mountain, Duhok Governorate, Kurdistan, NE Iraq: Geochemistry, mineralogy and origin. *Arabian Journal of Geosciences*, 9, p.473.

Mohialdeen, I.M., and Raza, S.M., 2013. Inorganic geochemical evidence for the depositional facies associations of the Upper Jurassic Chia Gara Formation in NE Iraq. *Arabian Journal of Geosciences*, 6, pp.4755-4770.

Murray, R.W., Ten Brink, M.R.B., Gerlach, D.C., Russ III, G.P., and Jones, D.L., 1991. Rare earth, major, and trace elements in chert from the Franciscan Complex and Monterey Group, California: Assessing REE sources to fine-grained marine sediments. *Geochimica et Cosmochimica Acta*, 55, pp.1875-1895.

Mustafa, R.K., and Tobia, F.H., 2020. Geochemical application in unraveling paleoweathering, provenance and environmental setting of the shale from Chia Gara Formation, Kurdistan Region, Iraq. *The Iraqi Geological Journal*, 53, pp.90-116.

Omar, N., Mccann, T., Al-Juboury, A.I., and Franz, S.O., 2020. Petrography and geochemistry of the middle-upper Jurassic Banik section, Northernmost Iraq-implications for palaeoredox, evaporitic and diagenetic conditions. *Neues Jahrbuch für Geologie und Paläontologie Abhandlungen*, 297, pp.125-152.

Omar, N., Mccann, T., Al-Juboury, A.I., Ustinova, M.A., and Sharezwri, A.O., 2022. Early jurassic-early cretaceous calcareous nannofossil biostratigraphy and geochemistry, Northeastern Iraqi Kurdistan: Implications for paleoclimate and paleoecological conditions. *Geosciences,* 12, p.94.

Ozkan, A., 2019. Geochemical features of rare earth elements in the dolomites of the bozdağ formation (early silurian-middle devonian) from Söğütözü-Ladik (Konya/Turkey) area. *International Journal of Engineering Science*, 8, pp.30-46.

Ozyurt, M., Kirmaci, M.Z., Al-Aasm, I., Hollis, C., Tasli, K., and Kandemir,xR., 2020. REE characteristics of lower cretaceous limestone succession in gumushane, NE Turkey: Implications for ocean paleoredox conditions and diagenetic alteration. *Minerals*, 10, p.683.

Ozyurt, M., Kirmaci, M.Z., and Al-Aasm, I.S., 2019. Geochemical characteristics of Upper Jurassic-lower cretaceous platform carbonates in Hazine Magara, Gumushane (Northeast Turkey): Implications for dolomitization and recrystallization. *Canadian Journal of Earth Sciences*, 56, pp.306-321.

Pattan, J., Masuzawa, T., Borole, D., Parthiban, G., Jauhari, P., and Yamamoto, M., 2005. Biological productivity, terrigenous influence and noncrustal elements supply to the Central Indian Ocean Basin: Paleoceanography during the past□ 1 Ma. *Journal of Earth System Science*, 114, pp.63-74.

Randive, K., 2013. *Elements of Geochemistry, Geochemical Exploration and Medical Geology*. Research Publishing Service, Singapore.

Shields, G., and Stille, P., 2001. Diagenetic constraints on the use of cerium anomalies as palaeoseawater redox proxies: An isotopic and REE study of Cambrian phosphorites. *Chemical Geology*, 175, pp.29-48.

Taylor, S.R., and Mclennan, S.M., 1985. *The Continental Crust: Its Composition and Evolution.* Blackwell Scientific Publications, United Kingdom.

Tobia, F.H., Al-Jaleel, H.S., and Ahmad, I.N., 2019. Provenance and depositional environment of the Middle-Late Jurassic shales, Northern Iraq. *Geosciences Journal*, 23, pp.747-765.

Tobia, F.H., and Shangola, S.S., 2016. Mineralogy, geochemistry, and depositional environment of the beduh shale (lower triassic), Northern Thrust Zone, Iraq. *Turkish Journal of Earth Sciences,* 25, pp.367-391.

Tostevin, R., Shields, G.A., Tarbuck, G.M., He, T., Clarkson, M.O., and Wood, R.A., 2016. Effective use of cerium anomalies as a redox proxy in carbonate-dominated marine settings. *Chemical Geology,* 438, pp.146-162.

Tribovillard, N., Algeo, T.J., Lyons, T., and Riboulleau, A., 2006. Trace metals as paleoredox and paleoproductivity proxies: An update. *Chemical geology*, 232, pp.12-32.

Wang, F., Chen, R., Liang, Q., Chang, X., Tian, J., and Deng, X., 2020. Geochemical characteristics and depositional environments of mudstones from the Triassic Zhifang Formation in the Tongchuan Area, Southern Ordos Basin, China. *Geological Journal*, 55, pp.3857-3869.

Wilde, P., Quinby-Hunt, M.S., and Erdtmann, B.D., 1996. The whole-rock cerium anomaly: A potential indicator of eustatic sea-level changes in shales of the anoxic facies. *Sedimentary Geology*, 101, pp.43-53.

Xiao, B., Guo, D., Li, S., Xiong, S., Jing, Z., Feng, M., Fu, X., and Zhao, Z., 2024. Rare earth element characteristics of shales from Wufeng-Longmaxi formations in deep-buried areas of the Northern Sichuan Basin, Southern China: Implications for provenance, depositional conditions, and paleoclimate. *ACS Omega*, 9, pp.2088-2103.

Xu, L., Huang, S., Sun, M., Wen, Y., Chen, W., Zhang, Y., Luo, F., and Zhang, H., 2023. Palaeoenvironmental evolution based on elemental geochemistry of the Wufeng-Longmaxi shales in Western Hubei, Middle Yangtze, China. *Minerals*, 13, p.502.

Yu, W., Wang, F., Gong, L., Hu, J., Ma, Z., Wang, J., Wu, J., and Xiao, Y., 2023. Paleoenvironmental, paleoclimatic, and tectonic implications of the Yanghugou formation in the Western margin of the Ordos Basin, China: Evidence from palynology and elemental geochemical characteristics. *Minerals,* 14, p.32.

Zhang, W., Yang, H., Yang, Y., Kong, Q., and Wu, K., 2008. Petrology and element geochemistry and development environment of Yanchang formation Chang-7 high quality source rocks in Ordos Basin. *Geochimica*, 37, pp.59-64.